THE JOURNAL OF PHYSICAL CHEMISTRY A

Article

Cite This: J. Phys. Chem. A XXXX, XXX, XXX−XXX

pubs.acs.org/JPCA

Vibrational Energy Relaxation: A Benchmark for Mixed Quantum−Classical Methods

Amber Jain and Joseph E. Subotnik*

Department of Chemistry, University of Pennsylvania, 231 South 34th Street, Philadelphia, Pennsylvania 19104, United States

ABSTRACT: We investigate the ability of mixed quantum−classical methods to capture the dynamics of vibrational energy relaxation. Several methods, including surface hopping, and Ehrenfest and symmetrical quasiclassical (SQC) dynamics, are benchmarked for the exactly solvable model problem of a harmonic oscillator bilinearly coupled to a bath of harmonic oscillators. Results show that, very often, one can recover accurate vibrational relaxation rates and detailed balance using simple mixed quantum−classical approaches. A few anomalous results do appear, however, especially regarding Ehrenfest and SQC dynamics.

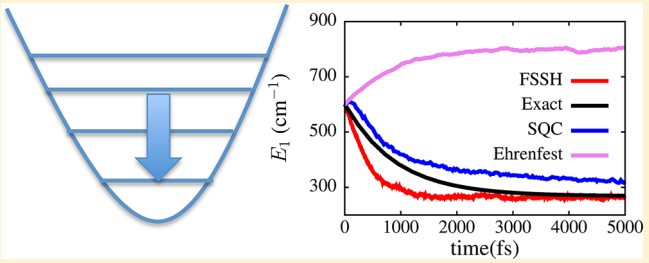

1. INTRODUCTION

Chemical reactions often lead to vibrationally hot products. Because vibrational energy relaxation (VER) of such hot products always competes with the opposite back reaction, understanding the rate and mechanisms of VER is critical for controlling a chemical reaction. Accordingly, the computation of VER rates has received immense attention in the literature.[1−4]

In practice, when studying VER, the key question is how does the environment affect VER? Often, quantum mechanical effects can play a significant role in determining the rate and mechanism of energy flow.[5−8] To analyze a large vibrational environment, exact nuclear dynamics is usually impossible: mixed quantum−classical dynamics are often the only possibility. However, because there is no unique way to embed a quantum system inside of a classical environment, the reliability of most such mixed quantum−classical methods can always be questioned.[9,10] Thus, in this work, we would like to investigate two popular but dissimilar mixed quantum−classical methods for computing VER rates: fewest switches surface hopping (FSSH)[11] and Miller's symmetrical quasiclassical (SQC)[12] method.

FSSH and SQC represent very different approaches for mixed quantum−classical dynamics. First consider FSSH. FSSH is a popular, stochastic tool for running dynamics that is a very rough, approximate solution to the quantum−classical Liouville equation (QCLE).[13,14] Nowadays, FSSH is one of the most popular choices for simulating mixed quantum−classical dynamics, and there is a significant literature calculating VER rates with FSSH (often obtaining rates within a factor of 2 compared to the experimental rates).[15−21] Theoretical investigations by Tully on reduced dimensional models have demonstrated that FSSH should capture VER rates qualitatively,[22] and furthermore, Tully and co-workers[23,24] and Corcelli and co-workers[25] have shown that FSSH obtains detailed balance approximately. Interestingly, however, Käb has argued that decoherence is essential for obtaining detailed balance when studying the vibrational relaxation of a harmonic oscillator bilinearly coupled to a bath of harmonic oscillators.[26] In ref 26, Käb also proposed a novel decoherence rate based on a Redfield-type quantum master equation. We will address Käb's results below.

Now, quite different from FSSH dynamics, SQC dynamics are smooth and based on a mean-field approximation. Building upon the early work of Meyer and Miller[27] and Stock and Thoss,[28] SQC dynamics require binning initial and final coordinates symmetrically. This symmetric binning procedure provides both a swarm of initial conditions (which leads to branching) and a means to quantize final coordinates (which ensures detailed balance in a thermal environment). To date, SQC has been studied for scattering problems[12] and the spin-Boson problem.[29] SQC has achieved some successes, especially for harmonic potentials (i.e., the spin-boson model), while some numerical instabilities also appear for anharmonic potentials.[30] To our knowledge, SQC has not yet been benchmarked for computing VER rates.

With this background in mind, the goal of this paper is to benchmark the FSSH and SQC methods for VER processes and identify the regimes of applicability for each method. Although almost certainly too simplistic, our model system will be a Hamiltonian comprising a harmonic oscillator bilinearly coupled to a bath of harmonic oscillators where a numerically exact solution is straightforward. Many years ago, Kohen, Stillinger, and Tully[22] analyzed a similar problem with only a system mode and one bath mode, and they found that Ehrenfest dynamics outperformed FSSH dynamics. Here, we wish to extend that earlier model and analyze the dynamical behavior with a true bath of harmonic modes. For the sake of completeness, we will also benchmark all results against Landau−Teller theory,[1] a standard tool for studying VER. These comparisons will provide detailed

Received: September 10, 2017
Revised: November 14, 2017

DOI: 10.1021/acs.jpca.7b09018
J. Phys. Chem. A XXXX, XXX, XXX−XXX

insights into the role of decoherence and frustrated hops in recovering detailed balance and rate constants within the FSSH algorithm.

Section 2 describes the model Hamiltonian. A brief overview of the FSSH and the SQC methodology is provided in Section 3, followed by results in Section 4 and a discussion in Section 5.

2. MODEL HAMILTONIAN

For this paper, our Hamiltonian will be very simple, a set of bilinearly coupled harmonic oscillators:[31]

$$H = H_s + H_b + V_c \tag{1}$$

$$H_s = \frac{p_1^2}{2m} + \frac{1}{2}m\omega_1^2 x_1^2 \tag{2}$$

$$H_b = \sum_{i=2}^{N}\left(\frac{p_i^2}{2m} + \frac{1}{2}m\omega_i^2 x_i^2\right) \tag{3}$$

$$V_c = \sum_{i=2}^{N} c_i x_i x_1 + \sum_{i=2}^{N}\frac{c_i^2}{2m\omega_i^2}x_1^2 \tag{4}$$

Here the same mass m is used for all degrees of freedom without loss of generality.

This model problem is exactly solvable (unlike the spin-boson problem) and has fewer parameters than the spin-boson problem (four relative to five). The couplings c_i are given by the bath spectral density $J(\omega)$:

$$J(\omega) = \frac{\pi}{2}\sum_i \frac{c_i^2}{m\omega_i}\delta(\omega - \omega_i) \tag{5}$$

Here we use an Ohmic spectral density, with an exponential cutoff:

$$J(\omega) = \eta m\omega e^{-\omega/\omega_c} \tag{6}$$

where η represents friction strength, and ω_c is related to the memory time as $\tau_{mem} \equiv \pi/2\omega_c$. We set $\omega_c = 650\ cm^{-1}$ (with $\tau_{mem} = 12$ fs). The simulations in this work are performed employing the spectral discretization scheme proposed by Makri[32]

$$\omega_i = -\omega_c \ln\left(\frac{i - \frac{3}{2}}{N-1}\right) \tag{7}$$

$$c_i = \omega_i\left[\frac{2\eta m\omega_c}{(N-1)\pi}\right]^{1/2} \tag{8}$$

We will focus on the population decay and the energy decay for mode 1 as it relaxes from the first vibrationally excited state to the ground state at time t. The population decay in the Heisenberg representation is given by

$$P(t) = \frac{1}{Q_b}\sum_{\vec{i}} e^{-\beta E_{\vec{i}}}\langle 1\vec{i}|P_0(t)|1\vec{i}\rangle \tag{9}$$

where $\beta = \frac{1}{k_B T}$ is the inverse temperature, Q_b is the bath partition function, $\vec{i}$ represents the set of all bath modes, and $E_{\vec{i}}$ is the corresponding bath energy

$$E_{\vec{i}} = \sum_{j=2}^{N}\hbar\omega_j\left(i_j + \frac{1}{2}\right) \tag{10}$$

P_0 in eq 9 is the projection operator on the ground vibrational state of mode 1:

$$P_0 = \sum_{\vec{i}} |0\vec{i}\rangle\langle 0\vec{i}| \tag{11}$$

Similar to the population, the energy in mode 1 is given by

$$E(t) = \frac{1}{Q_b}\sum_{\vec{i}} e^{-\beta E_{\vec{i}}}\langle 1\vec{i}|E_1(t)|1\vec{i}\rangle \tag{12}$$

with

$$E_1(t) = \hbar\omega_1\left[a_1(t)^\dagger a_1(t) + \frac{1}{2}\right] \tag{13}$$

Here a_1 ($a_1^\dagger$) is the annihilation (creation) operator. The exact solutions for $P(t)$ and $E(t)$ are outlined in Appendix A.

We note that the model Hamiltonian in eqs 1−4 is expected to be a challenging case for mixed quantum−classical methods for two inter-related reasons. First, Bader and Berne showed that, for this Hamiltonian, classical simulations recover exact quantum mechanical energy relaxation rates (although not population relaxation rates);[33] vice versa, they found that mixed quantum−classical dynamics performed less accurately (using their flavor of mixed quantum−classical dynamics). Thus, it is highly likely that our artificial separation between the quantum and classical modes (e.g., Ehrenfest, FSSH and SQC) might also lead to worse results. Second, here the primary pathway for energy relaxation is to transfer energy through a primary mode to a bath mode in resonance, and for the case of a high-frequency primary mode, a classical treatment of the resonant bath mode is questionable. Given these difficulties, this paper aims to identify those regimes (if any) where a direct quantum−classical simulation can accurately capture the relaxation process.

3. SIMULATION DETAILS

Below, we will compute and contrast VER rate constants using a number of different methodologies, especially FSSH and SQC. Each methodology has been described in detail elsewhere in the literature, but for the sake of completeness, we now provide a brief summary of each method (followed by the simulation details).

3.1. FSSH. The methodology for the fewest switches surface hopping approach can be found in refs 11 and 34. A recent efficient algorithm developed in our group[35] has been used for the present simulations. Here we treat the mode x_1 quantum mechanically, and all other bath modes (x_2, ..., x_N) are treated classically. Note that several quantum mechanical treatments of vibrational degrees of freedom have been performed in literature, including the work of Hammes-Schiffer and Tully,[36] Bastida and co-workers,[16−20] and Schubert and co-workers.[21]

For the model Hamiltonian in eqs 1−4, the adiabatic potential energy surfaces are always parallel. In particular, here we focus naturally on the collective bath coordinate $\zeta = \sum c_i x_i / \sum c_i$, which is directly coupled to the quantum subsystem. The potential energy surfaces are plotted in Figure 1 as a function of ζ.

For our simulations, the initial conditions for the classical degrees of freedom are chosen either from a (classical) Boltzmann distribution, or from a (quantum) Wigner distribution. The initial quantum state for mode x_1 is set to be the first vibrationally excited state (assuming the Hamiltonian is H_s). Because FSSH calculations are run in the adiabatic basis of $H = H_s + V_c$ (see eqs 1−4), a transformation back to a diabatic basis is

DOI: 10.1021/acs.jpca.7b09018
J. Phys. Chem. A XXXX, XXX, XXX−XXX

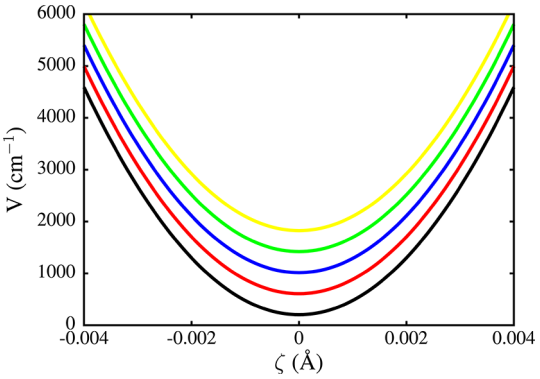

Figure 1. Vibrational adiabatic potential energy surfaces as a function of the collective bath coordinate $\zeta \equiv \sum c_i x_i / \sum c_i$ for the parameters ω_1 = 400 cm^{-1} and η = 2 ps^{-1}.

inevitably required to compute the vibrational state of x_1. Here, we follow ref 37 (method 3) for such a transformation.

A few words are now appropriate regarding decoherence and frustrated hops. First, regarding decoherence, starting from the work of Rossky, Bittner, Prezhdo, Schwartz, and Truhlar et al.,[38−40] it has long been conjectured that FSSH must be corrected with a decoherence rate proportional to the difference in forces between the different adiabats. This conjecture has been proven recently by comparing FSSH to the quantum−classical Liouville equation (QCLE).[13,14] Thus, for the present model, because the adiabats are always completely parallel, the decoherence probability is zero, and accordingly, we do not correct FSSH with any additional collapsing events in our simulations.

Second, regarding frustrated hops, there has been quite a long discussion in the literature regarding the fate of nuclear velocities after encountering a frustrated hop and whether or not to reverse velocities.[41−43] Recently, we have shown that, without velocity reversal, FSSH will not recover Marcus theory.[44] That being said, here we follow the recommendations of the Truhlar group,[45−48] who investigated the effects of frustrated hops extensively and recommend velocity reversal only when particles feel opposing forces from different adiabats. Hence, for this paper, we never change the velocity direction upon encountering a frustrated hop (i.e., the hop does not occur, and no other change is made on encountering a frustrated hop). Altogether, in one sense, the model Hamiltonian in eqs 1−4 is the simplest possible test case for FSSH dynamics.

Converged results for FSSH are obtained with 200 classical modes, and a classical time step of 0.5 fs. The quantum time step is chosen dynamically, following the procedure described in ref 35. The results are obtained by averaging over 1000 trajectories. All FSSH calculations are converged with respect to the number of vibrational states of x_1 (which usually requires 4 states). The vibrational eigenstates are computed using 30 discrete variable representation[49] functions ranging from $x_1 = -1.5$ Å to $x_1 = 1.5$ Å.

3.2. Ehrenfest and SQC Dynamics. Apart from surface hopping dynamics, the standard alternative is Ehrenfest dynamics, whereby trajectories move on mean-field surfaces. Because Ehrenfest dynamics do not obey detailed balance (i.e., they do not recover the correct equilibrium),[50−52] an improvement to Ehrenfest dynamics is the Cotton−Miller symmetrical quasiclassical (SQC) windowing approach.[53] Briefly, in this approach, the electronic amplitudes $\{c_j(t)\}$ are transformed into the action-angle variables $\{n_j(t), \theta_j(t)\}$:

$$c_j(t) = \sqrt{n_j(t)}\, e^{i\theta_j(t)} \tag{14}$$

The key insight of the SQC methodology is to symmetrically bin the initial and the final action around the quantum (integer) values. See ref 29 for more details.

Although Ehrenfest dynamics have been used often in the past to study vibrational relaxation,[50,51,54,55] to our knowledge, this paper represent the first benchmark of SQC for vibrational (as opposed to electronic) quantum degrees of freedom. For our model Hamiltonian, as will be shown below, the Ehrenfest method shows spurious nonexponential decay for populations, and sometimes an unphysical increase in energy. This unphysical behavior was observed previously by Käb.[51] That being said, however, we find that the SQC results often outperform Ehrenfest dynamics, and so, we will focus below on SQC. Ehrenfest results will be discussed in Section 5.2.

SQC simulations were performed with initial conditions for the classical degrees of freedom chosen either from a (classical) Boltzmann distribution or from a (quantum) Wigner distribution (i.e., the same as for the FSSH simulations). The initial action for the quantum variable is set to 1 for the first vibrational excited state of x_1 (using the Hamiltonian H_s in eq 1), and the action is set to 0 for all other states.

The SQC methodology also requires an adjustable parameter γ, which specifies the half-width of the binning window. We here set γ = 0.366 on the basis of the recommendations of the Miller group.[29] SQC simulations are performed with 1500 classical degrees of freedom, a nuclear time step of 0.5 fs, and a quantum time step of 0.005 fs. There are 10 000 trajectories used to average the results. As will be shown in Section 5.2, SQC results can depend strongly on the number of vibrational states of x_1 included. Unless otherwise stated, all results are shown with 4 vibrational states of x_1.

Ehrenfest dynamics were run with an initial Boltzmann distribution, 1000 classical degrees of freedom, a nuclear time step of 0.5 fs, and a quantum time step of 0.002 fs. Converged results are obtained with 15 eigenfunctions of H_s (see eq 1). An average over 1000 trajectories is reported for the Ehrenfest dynamics.

3.3. Classical Simulations. For completeness sake, we also report below results computed with the simplest method: classical dynamics.[56] These classical simulations are performed by integrating the Newtonian equations of motion with the velocity-Verlet algorithm. Initial conditions for the bath variables are chosen from a Boltzmann distribution. The initial coordinate and velocity for the mode x_1 (see eqs 1 and 2) are chosen using

$$x_1(t=0) = \sqrt{\frac{2E_1}{m\omega_1^2}}\cos(\theta) \tag{15}$$

$$v_1(t=0) = \sqrt{\frac{2E_1}{m}}\sin(\theta) \tag{16}$$

Here, θ is the angle variable chosen randomly between 0 and 2π, and $E_1 = (1 + \gamma_{cl})\hbar\omega_1$ is the initial energy in mode 1, where γ_{cl} is a random number between 0 and 1.

There is no unique way to quantize the population.[57,58] Here, we bin the classical action $n = E_1/\hbar\omega_1 - 0.5$ with a width of 1. That is, $n \in (-0.5, 0.5)$ is counted as the ground state, $n \in (0.5, 1.5)$ is counted as the first excited state, and so on.

Converged results for the classical simulations are obtained using 1000 bath modes and a time step of 0.5 fs. An average over 1000 trajectories is reported in the Results section.

DOI: 10.1021/acs.jpca.7b09018
J. Phys. Chem. A XXXX, XXX, XXX−XXX

3.4. Landau−Teller Theory. Within the vibrational dynamics community, for modeling VER, the default approach is the Landau−Teller formalism.[1] The rate constant in this formalism is given by Fermi's golden rule:

$$k_{10} = \frac{1}{\hbar^2}\int_{-\infty}^{\infty} \mathrm{d}t\ \mathrm{e}^{i\omega_1 t}\langle V_c^{10}(t)V_c^{01}\rangle_b \tag{17}$$

Here $V_c^{10} = \langle 1|V_c|0\rangle$ is an operator in the bath basis (see eq 4), and $\langle A\rangle_b$ represents the expectation value of an operator A in thermal equilibrium. Substituting eqs 2−4 into eq 17 gives the rate expression for the Hamiltonian under consideration

$$k_{LT} = \frac{1}{m}\frac{1}{\beta\hbar\omega_1}\frac{J(\omega_1)}{\omega_1}Q(\omega_1) \tag{18}$$

Here $Q(\omega_1)$ is the harmonic quantum correction factor[33] (QCF)

$$Q(\omega_1) = \frac{\beta\hbar\omega_1}{1-\mathrm{e}^{-\beta\hbar\omega_1}} \tag{19}$$

and $J(\omega)$ is the bath spectral density defined in eq 5.

Note that, for this paper, both the system and environment are harmonic so that we can evaluate the VER analytically with FGR. More generally, however, we usually assume that the system is harmonic, but the bath is anharmonic and the coupling need not be linear. In such a case, there is also a long-standing literature for evaluating FGR rates approximately with classical mechanics.[59−64] The inevitable question that arises is how to choose the appropriate QCF.[6] Estimates based on different choices of QCF can vary by several orders of magnitude.[6,65−67] Alternatively, Geva et al. have developed a semiclassical method to compute the quantum time correlation function.[7,68−73]

3.5. Numerically Exact Simulations. The case of a harmonic oscillator bilinearly coupled to a bath of harmonic oscillators can also be solved numerically exactly. Such a derivation based on Feynman's path integrals is presented in Appendix A. The final result for population decay is given by eq 37 and that for energy decay is given by eq 45.

Converged results are obtained with 500 bath modes. We use 10 time points for each simulation to obtain the decay of the population, and an exponential fit is performed thereafter to extract the rate constant.

4. RESULTS

Using the approaches discussed above, we will now compare vibrational relaxation rates (as measured by population and energy) and long-time thermal populations (focusing on whether detailed balance is recovered).

4.1. Population and Energy Decay as a Measure of Vibrational Relaxation. Figure 2 compares population relaxation rates as a function of variation in (a) the temperature, (b) the frequency of the primary mode ω_1, and (c) the friction strength η. For all results, the parameter regime is chosen such that $\hbar\omega_1 > k_BT$. Results are provided assuming either an initial Boltzmann or an initial Wigner distribution for the FSSH method. To avoid zero-point energy (ZPE) loss, classical data are presented with only Boltzmann initial coordinates. The classical results, as is well-known in literature,[33] disagree with the exact results when $k_BT \ll \hbar\omega_1$. Additionally, we find that initialization with either Boltzmann or Wigner distribution SQC results gives nearly identical rates, and hence, for clarity, only the results using the Boltzmann distribution will be reported.

Both the FSSH and SQC methods obtain decay rates within a factor of 2 compared to the exact results in a weak to moderate

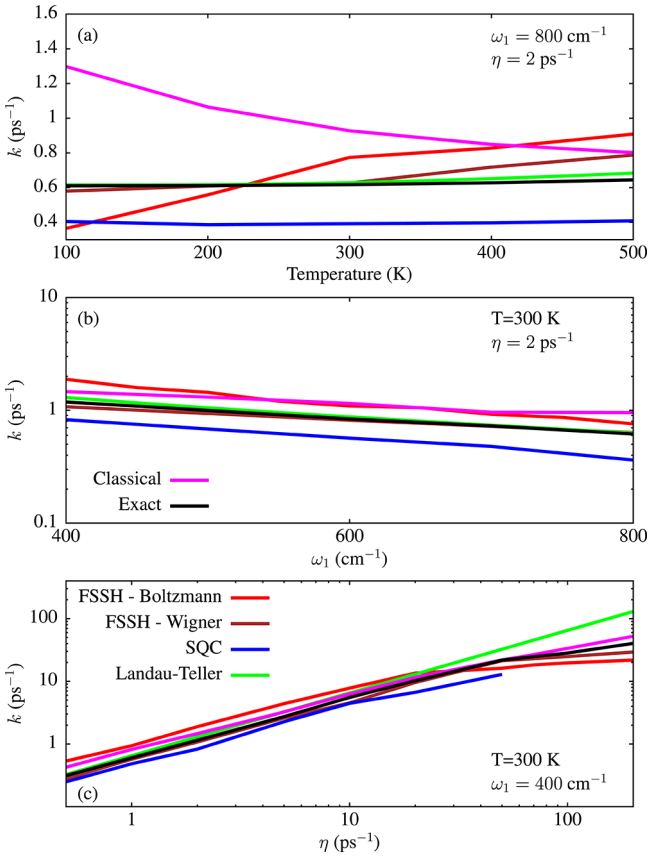

Figure 2. Population decay rates computed using various approaches. The Landau−Teller results are very close to the exact results except in the strong friction regime. FSSH rates are within a factor of 2 with an initial Boltzmann distribution across all of the parameters explored, and are nearly quantitative with an initial Wigner distribution. SQC results are nearly identical with initial Boltzmann or Wigner distribution, and for clarity's sake only Boltzmann results are reported. SQC rates are usually quite accurate and have the correct shape, except in the strong friction regime. This high friction anomaly is discussed in Section 5.3. All SQC data were computed using 4 vibrational states of x_1.

friction regime ($\eta/\omega_1 < 1$). In the weak coupling regime, SQC also recovers the correct trends. In the strong friction regime ($\eta/\omega_1 > 1$), however, we see deviations in the quality of results as obtained from the various approaches; see Figure 2c. Here, LT results show meaningful deviations, which might be expected since Fermi's golden rule is not applicable in the strong friction regime. FSSH results remain in good agreement with the exact results (within a factor of 2). SQC results become erratic at high friction. This behavior will be discussed in Section 5.3.

Figure 2 also highlights the role of zero-point energy for the bath modes. The FSSH results are in quantitative agreement with the exact results if an initial Wigner distribution is used. That being said, however, the FSSH errors are larger (up to a factor of 2) if we substitute a Boltzmann distribution for the Wigner distribution, which gives us a rough estimate of the importance of zero-point energy here. We emphasize that, for the FSSH calculations here, there is no leakage of zero-point energy from the bath modes (while using a Wigner distribution) over the time scales of the population relaxation, almost certainly due to the harmonic nature of the potential investigated here; most importantly, the bath mode in resonance with the system does not leak energy. More generally, we expect ZPE leakage will lead

DOI: 10.1021/acs.jpca.7b09018
J. Phys. Chem. A XXXX, XXX, XXX−XXX

to a deterioration in the quality of FSSH dynamics; using an initial Wigner distribution is obviously not a sinecure.[74−76]

Finally, before concluding this subsection, we plot the energy decay rates in Figure 3. The classical results here are nearly

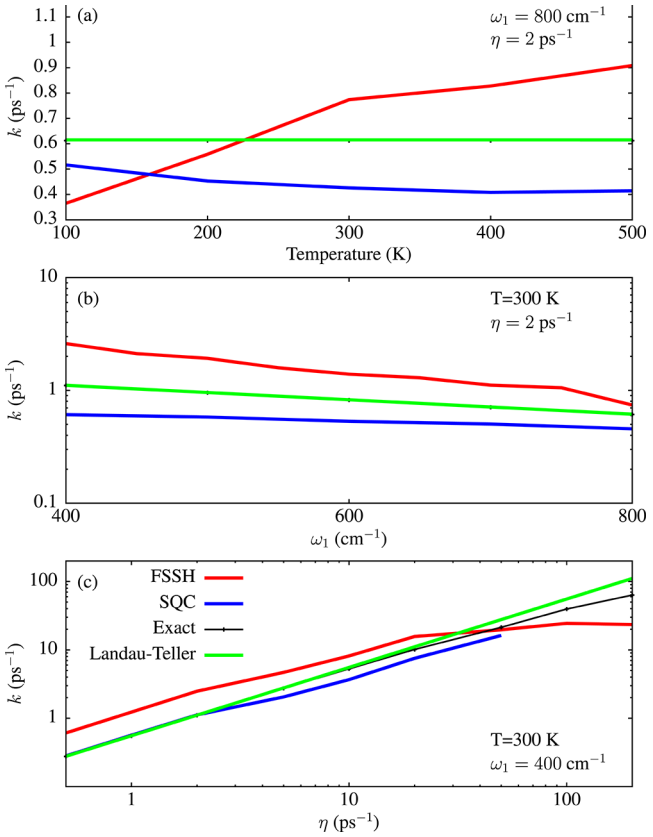

Figure 3. Comparison of energy decay rates computed using various methods. The classical results are not shown for clarity since the classical rates are in near quantitative agreement with the exact results. FSSH and SQC results are within a factor of 2 compared to the exact results, similar to the population decay rates shown in Figure 2. The SQC method shows spurious nonexponential behavior in the strong friction regime, which is discussed in detail in Section 5.3. The SQC results are computed with 4 vibrational states of x_1.

identical to the exact results (as is known in literature),[33] and are not shown for clarity. The SQC results are reported with 4 vibrational states, and inclusion of higher excited vibrational states would actually change the dynamics (as discussed in Section 5.2). The results for the energy decay follow the same trends as that of population decay: Both FSSH and SQC rates are within a factor of 2 compared to the exact results (except for the strong friction regime, where SQC shows nonexponential behavior).

4.2. Long-Time Population and Detailed Balance. We next focus our attention on equilibrium populations, shown in Figure 4. The classical results give the naive Boltzmann answer (which must be exact in the limit of weak coupling)

$$P_0^{\mathrm{B}} = \frac{1}{1 - \mathrm{e}^{-\beta\hbar\omega_1}} \tag{20}$$

Here, we report the SQC results with 4 vibrational x_1 states. The effects of higher excited vibrational states will be discussed in Section 5.2.

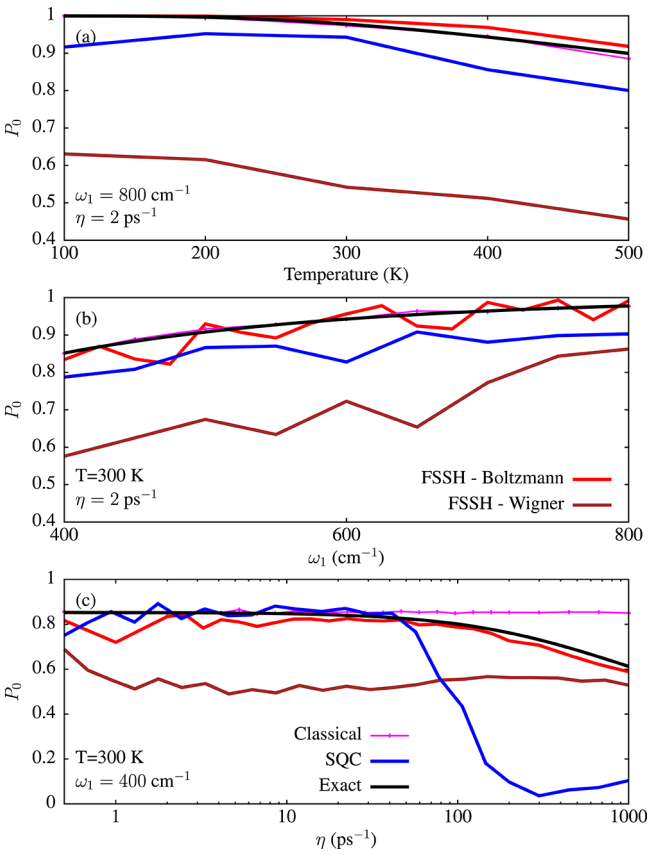

Figure 4. Comparison of equilibrium population computed using various approaches. FSSH satisfies detailed balance across all regimes to a very good approximation. The SQC results (computed with 4 vibrational states) do well for weak coupling, but break down for the strong friction regime. See Section 5.3. Inclusion of more than 4 vibrational states can also alter the SQC dynamics, as discussed in detail in Section 5.2.

4.2.1. Weak Coupling Limit. In the weak coupling limit, both FSSH and SQC are reasonably accurate. FSSH slightly outperforms SQC: While FSSH is in near quantitative agreement with the exact results, SQC is roughly 10% off. Note, though, that if one initializes the FSSH dynamics with a Wigner distribution, the quality of the results is far worse (although the population decay rate constants were in quantitative agreement, see Figure 2). Here, the bath would incorrectly reach a larger (and nonuniform) temperature because of zero-point energy. Thus, our results agree with the general wisdom regarding zero-point energy effects: Inclusion of such zero-point energy improves early time dynamics, but leads to incorrect populations at long times.[74−76]

4.2.2. Strong Coupling Limit. In the strong friction regime ($\eta > \omega_1$), the Boltzmann population is no longer accurate (of course). Here, however, we observe something curious: FSSH still captures the correct population in Figure 4c. By contrast, the SQC results (both for rates as well as thermal populations) fail in the strong friction regime. These phenomena will be discussed at length in Section 5.3.

5. DISCUSSION

5.1. Differences between our FSSH Results and the Predictions of Käb. The broad range of regimes investigated in Figures 2 and 4 shows that FSSH (without any decoherence) gets the rate constant within a factor of 2 of the exact results, and

DOI: 10.1021/acs.jpca.7b09018
J. Phys. Chem. A XXXX, XXX, XXX−XXX

obtains detailed balance nearly quantitatively. This result seems to be inconsistent with the previous work of Käb, who investigated the same model Hamiltonian and found that, without decoherence, FSSH does not obey detailed balance.[51]

The major difference between our approach and Käb's approach lies in the method used to compute diabatic populations. Whereas we use a mixed quantum−classical density approach (method 3 of ref 37), Käb uses the diabatic amplitude approach (method 2 of ref 37). At long times, the diabatic wavevector usually reaches an incorrect limit at high temperatures (even with decoherence; see Figures 1 and 2 of ref 37). In view of this well-known result, Käb's findings are not surprising.

That being said, FSSH performs quite well if we simply use the correct mixed quantum−classical density approach that connects FSSH dynamics with the quantum−classical Liouville equation.[13]

5.2. Dependence of Ehrenfest and SQC Dynamics on the Number of Highly Excited Vibrational States. Thus far, we have focused primarily on SQC with a relatively low number of vibrational states, and we have barely addressed Ehrenfest dynamics. To understand why this is so, we will now analyze energy decay for both Ehrenfest and SQC dynamics, paying special attention to how the results depend on the number of states included. In Figure 5, we plot energy decay for the

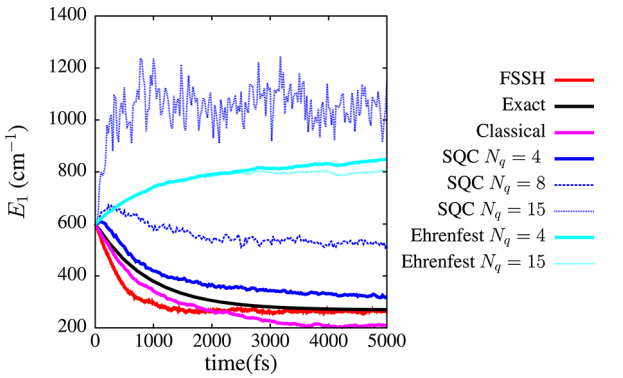

Figure 5. Energy decay as a function of time for $\omega_1 = 400$ cm^{-1}, $\eta = 2$ ps^{-1}, and $T = 300$ K. Note the unphysical increase in energy computed using the Ehrenfest method. The classical approach decays asymptotically to the incorrect energy. This failure at short times can be modeled analytically. See Appendix B. FSSH decays to approximately the correct limit, though the decay rate for FSSH is about a factor of 2 faster compared to the exact result. The SQC results vary significantly when the number of vibrational states of x_1 is increased from 4 to 15; for physical results one must run SQC with only a handful of states.

following set of parameters: $\omega_1 = 400$ cm^{-1}, $\eta = 2$ ps^{-1}, and $T = 300$ K. Note that the Ehrenfest dynamics are completely unphysical, as the energy of the high-frequency mode increases (rather than relaxes) in time, consistent with the observations of Käb.[50,51] To understand the origins of this unphysical increase in energy, in Appendix B we derive a short time rate expression for population and energy relaxation rates according to Ehrenfest dynamics. This analysis recovers the well-known result that Ehrenfest dynamics do not obey detailed balance (see eq 61) in contrast to FGR results, and as a consequence, one can show that the energy in the primary mode increases linearly at short times (see eq 67). Figure 7 plots Ehrenfest simulations and highlights the incorrect behavior at short times.

The shortcomings of the Ehrenfest dynamics can be partly corrected by the symmetrical windowing binning procedure of the SQC method. When a relatively small number of states is included ($N_q = 4$), the SQC approach gives nearly the correct result. However, when the number of vibrational states increases, SQC shows erroneous behavior. This strongly suggests that, for the problem of vibrational relaxation, one must be very careful in choosing the number of vibrational states: Including quantum states with large energy (much higher than thermal energy) can adversely affect the quality of the predicted dynamics. In short, the more vibrational states that are included, the larger the likelihood is that the dynamics of low-lying energetic states will be contaminated by zero-point energy loss from the high-lying energetic states.

5.3. Anomalies of the Large Friction Limit. Before concluding, we must now discuss the behavior of FSSH and SQC in the large friction limit (see Figures 2−4), where the adiabatic-to-diabatic transformation is far from the identity. Even though this parameter regime may be somewhat unphysical, insofar as one can question how to prepare the initial state experimentally, analyzing the behavior of semiclassical methods in this regime will be helpful for understanding how and when different methods fail. In particular, as noted above, FSSH behaves stably in this regime whereas SQC does not. To understand this dichotomy, consider first the FSSH algorithm. At equilibrium, most population resides on the lower adiabat, which is of course consistent with FSSH dynamics. Thus, to compute a diabatic population, one must merely use the correct FSSH surface information and the proper adiabatic-to-diabatic transformation. Thus, either the surface or density matrix interpretation of FSSH dynamics (i.e., approaches 1 and 3 from ref 37) would recover the correct, equilibrium diabatic population (as one might have expected). In Figure 6, we plot the population decay for weak and

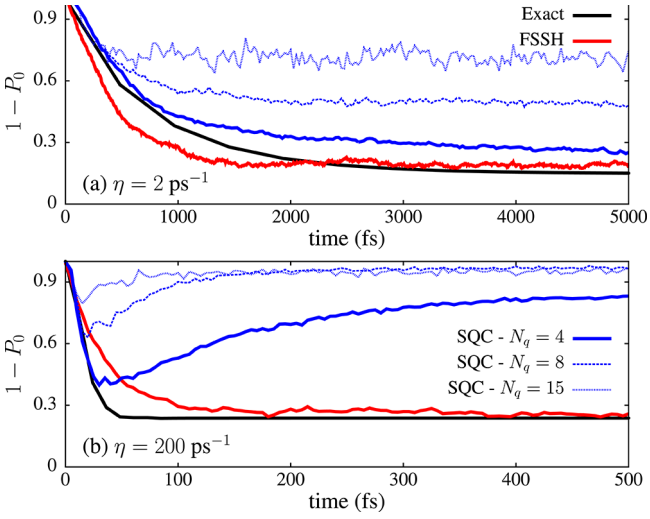

Figure 6. Population decay for $\omega_1 = 400$ cm^{-1}, $T = 300$ K, and $\eta = 2$ ps^{-1} and $\eta = 200$ ps^{-1}. The SQC method behaves well for weak friction with $N_q = 4$, but shows unphysical behavior at $\eta = 200$ ps^{-1}. FSSH (Boltzmann) decays correctly to the exact equilibrium result in both cases.

strong friction regimes. Note that, in both cases, FSSH performs fairly. (Here, we use the density matrix interpretation of surface hopping from ref 37, for consistency.)

Finally, consider SQC dynamics. According to SQC dynamics, one must bin the final result according to the action (see eq 14) in the observed basis. In the high friction regime, the diabatic basis is strongly coupled and might even be unphysical. For this

DOI: 10.1021/acs.jpca.7b09018
J. Phys. Chem. A XXXX, XXX, XXX−XXX

reason, SQC dynamics likely fail. In practice, note that, in Figure 6, SQC dynamics show spurious nonexponential behavior in this strong friction regime, so that the failures of SQC are quite obvious and likely can be avoided. In the future, it would be interesting to learn whether or not such unphysical behavior can be avoided by working in one basis and measuring in another (as in ref 77). It might also be interesting to study these dynamics as a function of the binning window because, as the window shrinks to zero, one must recover detailed balance if the bath modes do not include zero-point energy.[30]

Perhaps most interestingly, Figure 6 also highlights the dependence of SQC dynamics on the number of x_1 vibrational states (N_q). Although the short-term decay is not very sensitive, the long-term populations change significantly with N_q. SQC predicts an incorrect ground state thermal population because highly excited vibrational states acquire much higher population than the correct Boltzmann population. A future line of study must investigate how to choose the optimal number of vibrational states.

Lastly, for the skeptical reader, we want to emphasize that the conclusions from this paper are far from obvious. In a previous publication (Figure 7 of ref 30), we studied FSSH and SQC dynamics for a spin-boson model in a highly coupled (and unphysical) basis. For such a case, we previously found the exact opposite behavior; namely, we found that FSSH behaved poorly and suffered enormously from "recoherence" problems whereas the SQC algorithm performed quite well. (The exact dynamics are now reported in a recent Faraday discussions.)[78] For the moment, we conclude only that when making measurements in a strongly coupled basis, neither SQC nor FSSH may be reliable in general.

6. CONCLUSIONS

We have benchmarked two quantum−classical methods, FSSH and SQC, for their ability to capture vibrational energy relaxation. Our simple choice of Hamiltonian has been a model problem comprising a harmonic oscillator bilinearly coupled to a bath of harmonic oscillators, for which numerically exact results can be evaluated. We have explored the system dynamics as a function of temperature, the frequency of the primary mode, and the friction strength. Our results are as follows:

- On one hand, we find that FSSH rates are within a factor of 2, though there are variations in the errors of these rates; FSSH provides nearly quantitative agreement for long-time thermal populations. Our results contradict the earlier results of Käb[51] because we use the proper mixed quantum−classical density interpretation of FSSH dynamics.[37] The largest errors in the early time dynamics appear to be a consequence of the lack of zero-point energy effects for the bath modes. At the same time, we must also emphasize that if zero-point energy of the bath modes was to be included in simulations, FSSH would not capture detailed balance at long times.[30] At present, we may conclude only that the effects of zero-point energy must be carefully analyzed for the observable of interest.
- On the other hand, we find that SQC performs nearly as accurately as the FSSH method in the weak to moderate friction regime provided only a small number of quantum states are involved. In several cases, SQC outperforms FSSH. If quantum states with energies much higher than the thermal energy are included, however, one can obtain erroneous results; the SQC approach cannot be used for an arbitrary number of vibrational states. Finally, even with a small number of vibrational states, SQC behaves erratically in the strong friction regime, as the method can show spurious nonexponential decay for very large coupling. This latter failure may not be fatal, as one usually does not want to measure populations in a highly coupled basis.
- Lastly, we have shown that Ehrenfest dynamics can fail spectacularly and predict an unphysical increase in the energy for a system interacting with a cold bath. Our work highlights why detailed balance is essential for quantum dynamics simulations.

Looking forward, for more realistic simulations of VER and for stronger tests of the validity of mixed quantum−classical methods, the next step is clearly to explore nonharmonic potential energy surfaces. Here the multiphonon pathways to energy transfer can be significant, and the applicability of quantum−classical methods needs to be thoroughly benchmarked. For such problems, obviously, computing exact data can be difficult,[79] but this avenue must and will be pursued.

APPENDIX A: EXACT RESULTS

A.1. Population Decay

The population as a function of time is given by eq 9. This equation can be transformed into

$$P(t) = \frac{1}{Q_b} Tr[e^{-\beta H_b} P_1 e^{iHt} P_0 e^{-iHt}] \tag{21}$$

where Q_b is the partition function, $Tr[...]$ is the trace, and P_0 and P_1 are projection operators, projecting on the ground and first vibrational excited states of mode 1. Formally, these projection operators are given by

$$P_0 = \sum_{\vec{i}} |0\vec{i}\rangle\langle 0\vec{i}| \tag{22}$$

$$P_1 = \sum_{\vec{i}} |1\vec{i}\rangle\langle 1\vec{i}| \tag{23}$$

where $|\vec{ji}\rangle$ is the eigenket of $H_s + H_b$ (eqs 2 and 3).

We will evaluate eq 21 using the Feynman path integral approach. To start, we rewrite eq 21 as

$$P(t) = \int d\vec{w} \int d\vec{x} \int d\vec{y} \int d\vec{z} \left\langle \vec{x} \left| \frac{e^{-\beta H_b}}{Q_b} P_1 \right| \vec{y} \right\rangle \langle \vec{y}|e^{iHt}|\vec{z}\rangle\langle \vec{z}|P_0|\vec{w}\rangle\langle \vec{w}|e^{-iHt}|\vec{x}\rangle \tag{24}$$

where $|\vec{x}\rangle$, $|\vec{y}\rangle$, $|\vec{z}\rangle$, and $|\vec{w}\rangle$ denote the position eigenkets for the full system. Now, each element in eq 24 can be resolved as

DOI: 10.1021/acs.jpca.7b09018
J. Phys. Chem. A XXXX, XXX, XXX−XXX

$$\frac{1}{Q_b}\langle \vec{x}|e^{-\beta H_b}P_1|\vec{y}\rangle = \frac{2m\omega_1}{\hbar}\sqrt{\frac{m\omega_1}{\pi\hbar}}\prod_{i=2}^{N}\sqrt{\frac{m\omega_i[\cosh(\zeta_i)-1]}{\pi\hbar\sinh(\zeta_i)}}x_1y_1\exp\left[-\frac{m\omega_1}{2\hbar}(x_1^2+y_1^2)\right]$$
$$\prod_{i=2}^{N}\exp\left[-\frac{m\omega_i}{2\hbar\sinh(\zeta_i)}(\cosh(\zeta_i)(x_i^2+y_i^2))\right] \tag{25}$$

$$\langle \vec{y}|e^{iHt}|\vec{z}\rangle = \prod_{\alpha=1}^{N}\sqrt{\frac{im\tilde{\omega}_\alpha}{2\pi\hbar\sin(\tilde{\omega}_\alpha t)}}\prod_{i,j=1}^{N}\exp\left[\sum_\alpha U_{i\alpha}U_{j\alpha}\left(\frac{-im\tilde{\omega}_\alpha}{2\hbar\sin(\tilde{\omega}_\alpha t)}\right)(\cos(\tilde{\omega}_\alpha t)(y_iy_j+z_iz_j)-2y_iz_j)\right], \tag{26}$$

$$\langle \vec{z}|P_0|\vec{w}\rangle = \sqrt{\frac{m\omega_1}{\pi\hbar}}\exp\left[-\frac{m\omega_1}{2\hbar}(z_1^2+w_1^2)\right]\prod_{i=2}^{N}\delta(z_i-w_i) \tag{27}$$

$$\langle \vec{w}|e^{-iHt}|\vec{x}\rangle = \prod_{\alpha=1}^{N}\sqrt{\frac{-im\tilde{\omega}_\alpha}{2\pi\hbar\sin(\tilde{\omega}_\alpha t)}}\prod_{i,j=1}^{N}\exp\left[\sum_\alpha U_{i\alpha}U_{j\alpha}\left(\frac{im\tilde{\omega}_\alpha}{2\hbar\sin(\tilde{\omega}_\alpha t)}\right)(\cos(\tilde{\omega}_\alpha t)(w_iw_j+x_ix_j)-2z_ix_j)\right] \tag{28}$$

Here $\zeta_i = \beta\hbar\omega_i$, and the matrix U diagonalizes the Hessian F of the Hamiltonian (given in eqs 1−4); $\tilde{\omega}_\alpha$ is the corresponding eigenfrequency.

$$\mathbf{U}^\dagger\mathbf{F}\mathbf{U} = \mathbf{D} \tag{29}$$

$$D_{\alpha\alpha} = \hbar\tilde{\omega}_\alpha \tag{30}$$

Substituting eqs 25−28 in eq 24 gives the integral of the form:

$$P(t) = C(t)\int dq_1\int dq_2 \ldots \int dq_{3N+1}q_1q_{N+1}e^{-\mathbf{q}^T\mathbf{M}(\mathbf{t})\mathbf{q}} \tag{31}$$

with $\mathbf{M(t)}$ being a $3N+1$ by $3N+1$ matrix, $\{q_1, \ldots, q_N\} = \vec{x}$, $\{q_{N+1}, \ldots, q_{2N}\} = \vec{y}$, $\{q_{2N+1}, \ldots, q_{3N}\} = \vec{z}$, and $q_{3N+1} = w_1$. The normalization constant is

$$C(t) = \frac{1}{\pi^2}\left(\frac{m\omega_1}{\hbar}\right)^3\prod_{i=2}^{N}\left[\left(\frac{m\omega_i}{2\pi\hbar}\right)^{3/2}\sqrt{\frac{2(\cosh(\zeta_i)-1)}{\sinh(\zeta_i)}}\right]\frac{1}{\prod_{\alpha=1}^{N}\sin(\tilde{\omega}_\alpha t)} \tag{32}$$

To evaluate eq 31, consider the Gaussian integral

$$G(t) = \int dq_1\int dq_2 \ldots \int dq_{3N+1}e^{-\mathbf{q}^T\mathbf{M}(\mathbf{t})\mathbf{q}} \tag{33}$$

$$= \frac{\pi^{(3N+1)/2}}{\sqrt{Det[\mathbf{M}(\mathbf{t})]}} \tag{34}$$

where $Det[\mathbf{M(t)}]$ is the determinant of matrix $\mathbf{M(t)}$. It is now straightforward to see that $P(t)$ and $G(t)$ are related by

$$P(t) = -C(t)\frac{dG(t)}{dM_{1,N+1}} \tag{35}$$

$$= C(t)\frac{\pi^{(3N+1)/2}}{2Det[\mathbf{M}(\mathbf{t})]\sqrt{Det[\mathbf{M}(\mathbf{t})]}}\frac{dDet[\mathbf{M}(\mathbf{t})]}{dM_{1,N+1}} \tag{36}$$

For computational tractability, the expression 36 is recast as

$$P(t) = \frac{1}{2}\exp[\log(C(t)) + (3N+1)/2\log(\pi) - 1.5\log(Det[\mathbf{M}(\mathbf{t})]) + \log(A_{1,N+1})] \tag{37}$$

where $A_{1,N+1}$ is the $(1, N+1)$ cofactor of the matrix $\mathbf{M(t)}$. Equation 37 is the final expression that we use to numerically evaluate the exact decay of population.

A.2. Energy Decay

We begin evaluating the energy in mode 1 given by eq 12 by transforming to the normal mode representation (see eqs 29 and 30):

$$E_1(t) = \hbar\omega_1\left[\sum_{\alpha\beta}U_{1\alpha}U_{1\beta}a_\alpha^\dagger(t)a_\beta(t) + \frac{1}{2}\right] \tag{38}$$

$$= \hbar\omega_1\left[\sum_{\alpha\beta}U_{1\alpha}U_{1\beta}a_\alpha^\dagger a_\beta e^{i(\tilde{\omega}_\alpha-\tilde{\omega}_\beta)t} + \frac{1}{2}\right] \tag{39}$$

Here we have used the well-known result for a harmonic oscillator: $a_\alpha(t) = a_\alpha e^{-i\tilde{\omega}_\alpha t}$. Substituting eq 39 in eq 12 gives

$$E(t) = \hbar\omega_1\left[\sum_{\alpha\beta}U_{1\alpha}U_{1\beta}e^{i(\tilde{\omega}_\alpha-\tilde{\omega}_\beta)t}\frac{1}{Q_b}\sum_{\vec{i}}e^{-\beta E_{\vec{i}}}\langle 1\vec{i}|a_\alpha^\dagger a_\beta|1\vec{i}\rangle + \frac{1}{2}\right] \tag{40}$$

DOI: 10.1021/acs.jpca.7b09018
J. Phys. Chem. A XXXX, XXX, XXX−XXX

To simplify, we transform back to the Cartesian coordinates

$$\frac{1}{Q_b}\sum_{\vec{i}} e^{-\beta E_{\vec{i}}}\langle 1\vec{i}|a_\alpha^\dagger a_\beta|1\vec{i}\rangle = \frac{1}{Q_b}\sum_{\vec{i}}\sum_{jk} e^{-\beta E_{\vec{i}}}\langle 1\vec{i}|U_{j\alpha}U_{k\beta}a_j^\dagger a_k|1\vec{i}\rangle \tag{41}$$

$$= \frac{1}{Q_b}\sum_{\vec{i}}\sum_{j=2}^{N} e^{-\beta E_{\vec{i}}}U_{j\alpha}U_{j\beta}i_j + U_{1\alpha}U_{1\beta} \tag{42}$$

$$= \sum_{j=2}^{N} U_{j\alpha}U_{j\beta}\frac{e^{-\beta\hbar\omega_j}}{1+e^{-\beta\hbar\omega_j}} + U_{1\alpha}U_{1\beta} \tag{43}$$

Finally, substituting eq 43 in eq 40 gives

$$E(t) = \hbar\omega_1\left[\sum_{j=2}^{N}\sum_{\alpha\beta} U_{1\alpha}U_{j\alpha}U_{1\beta}U_{j\beta}e^{i(\tilde{\omega}_\alpha-\tilde{\omega}_\beta)t}\frac{e^{-\beta\hbar\omega_j}}{1+e^{-\beta\hbar\omega_j}} + \sum_{\alpha\beta} U_{1\alpha}^2U_{1\beta}^2 e^{i(\tilde{\omega}_\alpha-\tilde{\omega}_\beta)t} + \frac{1}{2}\right] \tag{44}$$

$$= \hbar\omega_1\left[\sum_{j=2}^{N}\left|\sum_\alpha U_{1\alpha}U_{j\alpha}e^{i\tilde{\omega}_\alpha t}\right|^2\frac{e^{-\beta\hbar\omega_j}}{1+e^{-\beta\hbar\omega_j}} + \left|\sum_\alpha U_{1\alpha}^2 e^{i\tilde{\omega}_\alpha t}\right|^2 + \frac{1}{2}\right] \tag{45}$$

Equation 45 is the final equation we use to compute energy as a function of time.

APPENDIX B: ESTIMATE FOR VER ACCORDING TO EHRENFEST DYNAMICS

Here we present an analytic approach that can explain the unphysical increase in energy predicted by Ehrenfest dynamics (see Figure 5). Within the Ehrenfest formalism, as noted in Section 3.2, we treat mode 1 quantum mechanically and the rest of the bath classically. Hence, we rewrite the Hamiltonian in eqs 1−4 as

$$H = H_s + H_b + V_c \tag{46}$$

$$H_s = \sum_n \epsilon_n|n\rangle\langle n| \tag{47}$$

$$H_b = \sum_{i=2}^{N}\left(\frac{p_i^2}{2m} + \frac{1}{2}m\omega_i^2x_i^2\right) \tag{48}$$

$$V_c = \sum_{i=2}^{N} c_ix_i\hat{x}_1 + \sum_{i=2}^{N}\frac{c_i^2}{2m\omega_i^2}\hat{x}_1^2 \tag{49}$$

where $|n\rangle$ is the eigenfunction of H_s, $\epsilon_n = \left(n+\frac{1}{2}\right)\hbar\omega_1$, and $\hat{x}_1$ is the position operator

$$\hat{x}_1 = \sqrt{\frac{\hbar}{2m\omega_1}}\sum_n \sqrt{n+1}\,(|n\rangle\langle n+1| + |n+1\rangle\langle n|) \tag{50}$$

Now, in order to compute population and energy dynamics, we will make two approximations: (a) we assume the validity of first order perturbation theory (i.e., we assume weak coupling), and (b) we neglect transitions from state n to $n \pm 2$ (i.e., we ignore the $\hat{x}_1^2$ term in eq 49). Under these approximations, if the system is initially prepared in state n, the quantum amplitude in state $n+1$ at time t is then

$$d_{n+1}(t) = \frac{-i}{\hbar}\langle n+1|\hat{x}_1|n\rangle\int_0^t dt' e^{i\omega_1t'}\left(\sum_{i=2}^{N} c_ix_i(t')\right) \tag{51}$$

For times that are much smaller than the reaction time constant, we can approximate each bath mode as an independent harmonic oscillator. That is

$$x_i(t) = x_i(0)\cos(\omega_it) + \frac{v_i(0)}{\omega_i}\sin(\omega_it) \tag{52}$$

with the correlation functions for $x_i(0)$ and $v_i(0)$ given by

$$\langle v_i(0)v_j(0)\rangle = \frac{k_BT}{m}\delta_{i,j} \tag{53}$$

$$\langle x_i(0)x_j(0)\rangle = \frac{k_BT}{m\omega_i^2}\delta_{i,j} \tag{54}$$

$$\langle x_i(0)v_j(0)\rangle = 0 \tag{55}$$

Substituting eq 52 into eq 51 [and ignoring terms with frequency $(\omega_1+\omega_i)$] gives

$$d_{n+1}(t) = \frac{\langle n+1|\hat{x}_1|n\rangle}{\hbar}\sum_{i=2}^{N} c_i\left[x_i(0) + i\frac{v_i(0)}{\omega_i}\right]\frac{\sin[(\omega_1-\omega_i)t/2]}{\omega_1-\omega_i}e^{i(\omega_1-\omega_i)t/2} \tag{56}$$

Within the Fermi golden rule formalism, the rate of transition from state n to state $n+1$ is approximated by

$$k_{n,n+1} = \frac{d}{dt}\lim_{t\to\infty}\langle|d_{(n+1)}(t)|^2\rangle_b \tag{57}$$

where $\langle\ldots\rangle_b$ is the thermal average over the bath degrees of freedom. Substituting eq 56 into eq 57, and utilizing eqs 53−55 together with the identity

$$\lim_{t\to\infty}\frac{\sin^2[(\omega_1-\omega_i)t/2]}{(\omega_1-\omega_i)^2} = \frac{\pi t}{2}\delta(\omega_1-\omega_i) \tag{58}$$

gives

$$k_{n,n+1} = \frac{1}{\hbar^2}|\langle n+1|\hat{x}_1|n\rangle|^2\sum_i c_i^2\left[\frac{2k_BT}{m\omega_i^2}\right]\frac{\pi}{2}\delta(\omega_1-\omega_i) \tag{59}$$

$$= (n+1)\frac{1}{m}\frac{1}{\beta\hbar\omega_1}\frac{J(\omega_1)}{\omega_1} \tag{60}$$

Equation 60 is the Landau−Teller result (eq 18) with a quantum correction factor of 1. Note that this rate constant does not obey detailed balance. If we calculate $k_{n+1,n}$ in the same fashion, we will find

$$k_{n+1,n} = k_{n,n+1} \tag{61}$$

$$= (n+1)k_{0,1} \tag{62}$$

Thus, suppose we wish to use a master equation to describe the population dynamics (ignoring any contribution from off-diagonal terms of the density matrix):

$$\dot{P}_n = \sum_m -k_{n,m}P_n + k_{m,n}P_m \tag{63}$$

If we then evaluate the decay of the energy E, where

DOI: 10.1021/acs.jpca.7b09018
J. Phys. Chem. A XXXX, XXX, XXX−XXX

$$\dot{E} = \sum_n \epsilon_n \dot{P}_n \tag{64}$$

and substitute eq 63 into eq 64 and use the identities in eq 61 and eq 62, we will find

$$\dot{E} = \sum_n \hbar\omega_1 P_n (k_{n+1,n} - k_{n,n-1}) \tag{65}$$

$$= \hbar\omega_1 k_{1,0} \tag{66}$$

$$= \frac{k_B T}{m} \frac{J(\omega_1)}{\omega_1} \tag{67}$$

Equation 67 provides a very strange conclusion: within the weak coupling regime, the energy of the primary mode always increases linearly. This gain in energy is a consequence of the fact that the rate constants in eq 60 (and hence the populations) do not obey detailed balance (which is well-known for Ehrenfest dynamics).

To prove the validity of the master equation approach above, Figure 7a plots the energy decay as obtained from Ehrenfest dynamics versus the predictions of eqs 63 and 67. The master equation approach matches well with the Ehrenfest simulations at short times (about 200 fs) confirming our expectations regarding the unphysical behavior predicted by mean-field dynamics. At longer times, eq 52 no longer matches Ehrenfest dynamics as the energies of bath modes change. Furthermore, in Figure 7b, we plot the relative populations of the different vibrational states $n = 0, 1, 2$. Note that, at long times, $n = 0$ and $n = 2$ have equal populations (approximately). Further, to confirm that the gain in system energy is indeed coming from the bath, in Figure 7c, we plot the energy of the system (H_s in eq 47) and the bath (H_b in eq 48) for $\omega_1 = 400$ cm^{-1}. We observe a gain of roughly 150 cm^{-1} of energy by the system and an equal loss by the bath, thus confirming that the energy is indeed transferred from the system to the bath.[80] This numerical example is a strong reminder that propagating dynamics according to a protocol that does not return detailed balance is very risky.

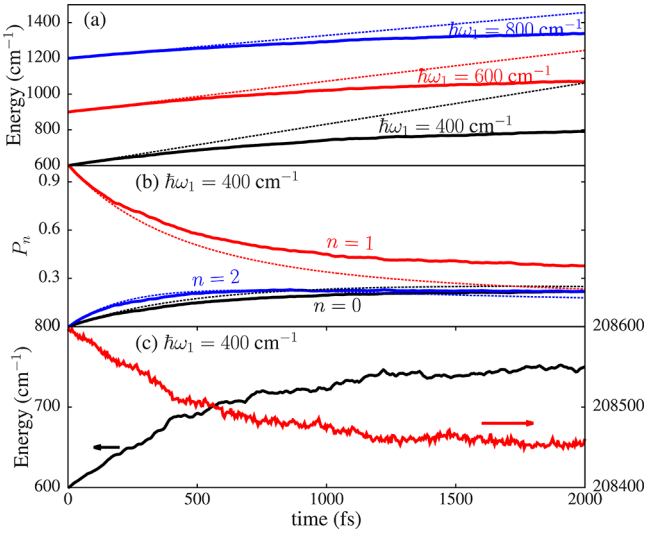

Figure 7. (a) Energy of the system for different frequencies of the primary mode. (b) Population of various states $n = 0$, 1, and 2 (for $\omega_1 = 400$ cm^{-1}). (c) Energy of the system and the bath (for $\omega_1 = 400$ cm^{-1}). For all simulations, $T = 300$ K, and $\eta = 2$ ps^{-1}. Solid lines are Ehrenfest results, and the dashed lines are master equation results. For part c, the system energy (black) is plotted according to the scale on the left y-axis, and the bath energy (red) is plotted according to the scale on the right y-axis. Overall, our master equation results are in good agreement with the Ehrenfest simulations until about 200 fs, confirming the theoretical analysis above.

AUTHOR INFORMATION

Corresponding Author

*E-mail: subotnik@sas.upenn.edu.

ORCID

Amber Jain: 0000-0002-8003-8716

Notes

The authors declare no competing financial interest.

ACKNOWLEDGMENTS

This material is based upon work supported by the (U.S.) Air Force Office of Scientific Research (USAFOSR) PECASE award under AFOSR Grant No. FA9950-13-1-0157.

REFERENCES

(1) Owrutsky, J. C.; Raftery, D.; Hochstrasser, R. M. Vibrational relaxation dynamics in solutions. *Annu. Rev. Phys. Chem.* **1994**, *45*, 519−555.

(2) Stratt, R. M.; Maroncelli, M. Nonreactive dynamics in solution: The emerging molecular view of solvation dynamics and vibrational relaxation. *J. Phys. Chem.* **1996**, *100*, 12981−12996.

(3) Harris, C. B.; Smith, D. E.; Russell, D. J. Vibrational relaxation of diatomic molecules in liquids. *Chem. Rev.* **1990**, *90*, 481−488.

(4) Sibert, E. L.; Ramesh, S. G.; Gulmen, T. S. Vibrational relaxation of OH and CH fundamentals of polar and nonpolar molecules in the condensed phase. *J. Phys. Chem. A* **2008**, *112*, 11291−11305.

(5) Poulsen, J. A.; Rossky, P. J. Path integral centroid molecular-dynamics evaluation of vibrational energy relaxation in condensed phase. *J. Chem. Phys.* **2001**, *115*, 8024−8031.

(6) Skinner, J. L.; Park, K. Calculating vibrational energy relaxation rates from classical molecular dynamics simulations: Quantum correction factors for processes involving vibration-vibration energy transfer. *J. Phys. Chem. B* **2001**, *105*, 6716−6721.

(7) Shi, Q.; Geva, E. Semiclassical theory of vibrational energy relaxation in the condensed phase. *J. Phys. Chem. A* **2003**, *107*, 9059−9069.

(8) Leitner, D. M. Quantum localization and protein-assisted vibrational energy flow in cofactors. *New J. Phys.* **2010**, *12*, 085004.

(9) Kapral, R. Progress in the theory of mixed quantum-classical dynamics. *Annu. Rev. Phys. Chem.* **2006**, *57*, 129−157.

(10) Kapral, R. Quantum dynamics in open quantum-classical systems. *J. Phys.: Condens. Matter* **2015**, *27*, 073201.

(11) Tully, J. C. Molecular dynamics with electronic transitions. *J. Chem. Phys.* **1990**, *93*, 1061.

(12) Cotton, S. J.; Miller, W. H. Symmetrical windowing for quantum states in quasi-classical trajectory simulations. *J. Phys. Chem. A* **2013**, *117*, 7190−7194.

(13) Subotnik, J. E.; Ouyang, W.; Landry, B. R. Can we derive Tully's surface-hopping algorithm from the semiclassical quantum Liouville equation? Almost, but only with decoherence. *J. Chem. Phys.* **2013**, *139*, 214107.

(14) Kapral, R. Surface hopping from the perspective of quantum-classical Liouville dynamics. *Chem. Phys.* **2016**, *481*, 77−83.

(15) Li, S.; Thompson, W. H. Simulations of the vibrational relaxation of I2 in Xe. *J. Phys. Chem. A* **2003**, *107*, 8696−8704.

(16) Bastida, A.; Cruz, C.; Zúñiga, J.; Requena, A.; Miguel, B. Surface hopping simulation of the vibrational relaxation of I2 in liquid xenon using the collective probabilities algorithm. *J. Chem. Phys.* **2004**, *121*, 10611−10622.

(17) Bastida, A.; Zúñiga, J.; Requena, A.; Miguel, B. Molecular dynamics with quantum transitions study of the vibrational relaxation of

DOI: 10.1021/acs.jpca.7b09018
J. Phys. Chem. A XXXX, XXX, XXX−XXX

the HOD bend fundamental in liquid D2O. *J. Chem. Phys.* **2012**, *136*, 234507.
(18) Bastida, A.; Soler, M. A.; Zúñiga, J.; Requena, A.; Kalstein, A.; Fernández-Alberti, S. Hybrid quantum/classical simulations of the vibrational relaxation of the amide I mode of N-Methylacetamide in D2O solution. *J. Phys. Chem. B* **2012**, *116*, 2969−2980.
(19) Miguel, B.; Zúñiga, J.; Requena, A.; Bastida, A. Theoretical study of the temperature dependence of the vibrational relaxation of the H2O bend fundamental in liquid water and the subsequent distortion of the hydrogen bond network. *J. Phys. Chem. B* **2014**, *118*, 9427−9437.
(20) Miguel, B.; Zúñiga, J.; Requena, A.; Bastida, A. Relaxation pathways of the OD stretch fundamental of HOD in liquid H2O. *J. Chem. Phys.* **2016**, *145*, 244502.
(21) Schubert, A.; Falvo, C.; Meier, C. Mixed quantum-classical simulations of the vibrational relaxation of photolyzed carbon monoxide in a hemoprotein. *J. Chem. Phys.* **2016**, *145*, 054108.
(22) Kohen, D.; Stillinger, F. H.; Tully, J. C. Model studies of nonadiabatic dynamics. *J. Chem. Phys.* **1998**, *109*, 4713−4725.
(23) Parandekar, P. V.; Tully, J. C. Mixed quantum-classical equilibrium. *J. Chem. Phys.* **2005**, *122*, 094102.
(24) Schmidt, J. R.; Parandekar, P. V.; Tully, J. C. Mixed quantum-classical equilibrium: Surface hopping. *J. Chem. Phys.* **2008**, *129*, 044104.
(25) Sherman, M. C.; Corcelli, S. A. Thermal equilibrium properties of surface hopping with an implicit Langevin bath. *J. Chem. Phys.* **2015**, *142*, 024110.
(26) Käb, G. Fewest switches adiabatic surface hopping as applied to vibrational energy relaxation. *J. Phys. Chem. A* **2006**, *110*, 3197−3215.
(27) Meyer, H.; Miller, W. H. A classical analog for electronic degrees of freedom in nonadiabatic collision processes. *J. Chem. Phys.* **1979**, *70*, 3214−3223.
(28) Stock, G.; Thoss, M. Semiclassical description of nonadiabatic quantum dynamics. *Phys. Rev. Lett.* **1997**, *78*, 578−581.
(29) Cotton, S. J.; Miller, W. H. Symmetrical windowing for quantum states in quasi-classical trajectory simulations: Application to electronically non-adiabatic processes. *J. Chem. Phys.* **2013**, *139*, 234112.
(30) Bellonzi, N.; Jain, A.; Subotnik, J. E. An assessment of mean-field mixed semiclassical approaches: Equilibrium populations and algorithm stability. *J. Chem. Phys.* **2016**, *144*, 154110.
(31) Caldeira, A. O.; Leggett, A. J. Path integral approach to quantum Brownian motion. *Phys. A* **1983**, *121*, 587−616.
(32) Makri, N. The linear response approximation and its lowest order corrections: An influence functional approach. *J. Phys. Chem. B* **1999**, *103*, 2823−2829.
(33) Bader, J. S.; Berne, B. J. Quantum and classical relaxation rates from classical simulations. *J. Chem. Phys.* **1994**, *100*, 8359−8366.
(34) Subotnik, J. E.; Jain, A.; Landry, B.; Petit, A.; Ouyang, W.; Bellonzi, N. Understanding the surface hopping view of electronic transitions and decoherence. *Annu. Rev. Phys. Chem.* **2016**, *67*, 387−417.
(35) Jain, A.; Alguire, E.; Subotnik, J. E. An efficient, augmented surface hopping algorithm that includes decoherence for use in large-scale simulations. *J. Chem. Theory Comput.* **2016**, *12*, 5256−5268.
(36) Hammes-Schiffer, S.; Tully, J. C. Proton transfer in solution: Molecular dynamics with quantum transitions. *J. Chem. Phys.* **1994**, *101*, 4657.
(37) Landry, B. R.; Falk, M. J.; Subotnik, J. E. Communication: The correct interpretation of surface hopping trajectories: how to calculate electronic properties. *J. Chem. Phys.* **2013**, *139*, 211101.
(38) Schwartz, B. J.; Bittner, E. R.; Prezhdo, O. V.; Rossky, P. J. Quantum decoherence and the isotope effect in condensed phase nonadiabatic molecular dynamics simulations. *J. Chem. Phys.* **1996**, *104*, 5942−5955.
(39) Bedard-Hearn, M. J.; Larsen, R. E.; Schwartz, B. J. Mean-field dynamics with stochastic decoherence (MF-SD): A new algorithm for nonadiabatic mixed quantum/classical molecular-dynamics simulations with nuclear-induced decoherence. *J. Chem. Phys.* **2005**, *123*, 234106.
(40) Granucci, G.; Persico, M.; Zoccante, A. Including quantum decoherence in surface hopping. *J. Chem. Phys.* **2010**, *133*, 134111.
(41) Fang, J.-Y.; Hammes-Schiffer, S. Comparison of surface hopping and mean field approaches for model proton transfer reactions. *J. Chem. Phys.* **1999**, *110*, 11166−11175.
(42) Zhu, C.; Nobusada, K.; Nakamura, H. New implementation of the trajectory surface hopping method with use of the Zhu-Nakamura theory. *J. Chem. Phys.* **2001**, *115*, 3031−3044.
(43) Oloyede, P.; Mil'nikov, G.; Nakamura, H. Generalized trajectory surface hopping method based on the Zhu-Nakamura theory. *J. Chem. Phys.* **2006**, *124*, 144110.
(44) Jain, A.; Subotnik, J. E. Surface hopping, transition state theory, and decoherence. II. Thermal rate constants and detailed balance. *J. Chem. Phys.* **2015**, *143*, 134107.
(45) Jasper, A. W.; Hack, M. D.; Truhlar, D. G. The treatment of classically forbidden electronic transitions in semiclassical trajectory surface hopping calculations. *J. Chem. Phys.* **2001**, *115*, 1804−1816.
(46) Jasper, A. W.; Stechmann, S. N.; Truhlar, D. G. Fewest-switches with time uncertainty: A modified trajectory surface-hopping algorithm with better accuracy for classically forbidden electronic transitions. *J. Chem. Phys.* **2002**, *116*, 5424−5431.
(47) Jasper, A. W.; Truhlar, D. G. Improved treatment of momentum at classically forbidden electronic transitions in trajectory surface hopping calculations. *Chem. Phys. Lett.* **2003**, *369*, 60−67.
(48) Jasper, A. W.; Truhlar, D. G. Non-Born-Oppenheimer molecular dynamics of NaFH photodissociation. *J. Chem. Phys.* **2007**, *127*, 194306.
(49) Colbert, D. T.; Miller, W. H. A novel discrete variable representation for quantum mechanical reactive scattering via the Smatrix Kohn method. *J. Chem. Phys.* **1992**, *96*, 1982.
(50) Käb, G. Mean field Ehrenfest quantum/classical simulation of vibrational energy relaxation in a simple liquid. *Phys. Rev. E: Stat. Phys., Plasmas, Fluids, Relat. Interdiscip. Top.* **2002**, *66*, 046117.
(51) Käb, G. Statistical mechanics of mean field Ehrenfest quantum/classical molecular dynamics: The damped harmonic oscillator. *J. Phys. Chem. A* **2004**, *108*, 8866−8877.
(52) Parandekar, P. V.; Tully, J. C. Detailed balance in Ehrenfest mixed quantum-classical dynamics. *J. Chem. Theory Comput.* **2006**, *2*, 229−235.
(53) Miller, W. H.; Cotton, S. J. Communication: Note on detailed balance in symmetrical quasi-classical models for electronically non-adiabatic dynamics. *J. Chem. Phys.* **2015**, *142*, 131103.
(54) Terashima, T.; Shiga, M.; Okazaki, S. A mixed quantum-classical molecular dynamics study of vibrational relaxation of a molecule in solution. *J. Chem. Phys.* **2001**, *114*, 5663−5673.
(55) Bastida, A.; Cruz, C.; Zúñiga, J.; Requena, A.; Miguel, B. A modified Ehrenfest method that achieves Boltzmann quantum state populations. *Chem. Phys. Lett.* **2006**, *417*, 53−57.
(56) The reader may wonder about still another variant of classical dynamic with a semiclassical flavor: Why not simply run classical dynamics with quasiclassical initial conditions and then bin the classical action? This approach would be different from the SQC approach because we would not need to apply a Meyer−Miller mapping. This approach would be different from standard classical dynamics because we would include zero-point energy. This approach would be different from Ehrenfest dynamics because Ehrenfest and classical dynamics only agree (for a harmonic oscillator) for observables that are linear in position and momentum. Furthermore, this approach would be natural because, for a harmonic oscillator, one has an analytic form for the eigenvalues of the system. Nevertheless, we have not pursued this avenue here because this approach would not be as general for more complicated, anharmonic potentials.
(57) Bradley, K. S.; Schatz, G. C. A quasiclassical trajectory study of product energy and angular distributions in OH+ H2 (D2). *J. Phys. Chem.* **1994**, *98*, 3788−3795.
(58) Bonnet, L.; Rayez, J. Quasiclassical trajectory method for molecular scattering processes: necessity of a weighted binning approach. *Chem. Phys. Lett.* **1997**, *277*, 183−190.
(59) Rey, R.; Hynes, J. T. Vibrational energy relaxation of HOD in liquid D2O. *J. Chem. Phys.* **1996**, *104*, 2356−2368.
(60) Rostkier-Edelstein, D.; Graf, P.; Nitzan, A. Computing vibrational energy relaxation for high-frequency modes in condensed environments. *J. Chem. Phys.* **1997**, *107*, 10470−10479.

DOI: 10.1021/acs.jpca.7b09018
J. Phys. Chem. A XXXX, XXX, XXX−XXX

(61) Everitt, K.; Egorov, S.; Skinner, J. Vibrational energy relaxation in liquid oxygen. *Chem. Phys.* **1998**, *235*, 115−122.
(62) Lawrence, C.; Skinner, J. Vibrational spectroscopy of HOD in liquid D2. I. Vibrational energy relaxation. *J. Chem. Phys.* **2002**, *117*, 5827−5838.
(63) Gulmen, T. S.; Sibert, E. L. Vibrational energy relaxation of the OH stretch in liquid methanol. *J. Phys. Chem. A* **2004**, *108*, 2389−2401.
(64) Fujisaki, H.; Straub, J. E. Vibrational energy relaxation in proteins. *Proc. Natl. Acad. Sci. U. S. A.* **2005**, *102*, 6726−6731.
(65) Egorov, S.; Berne, B. Vibrational energy relaxation in the condensed phases: Quantum vs classical bath for multiphonon processes. *J. Chem. Phys.* **1997**, *107*, 6050−6061.
(66) Egorov, S.; Skinner, J. Semiclassical approximations to quantum time correlation functions. *Chem. Phys. Lett.* **1998**, *293*, 469−476.
(67) Egorov, S.; Everitt, K.; Skinner, J. Quantum dynamics and vibrational relaxation. *J. Phys. Chem. A* **1999**, *103*, 9494−9499.
(68) Shi, Q.; Geva, E. Vibrational energy relaxation in liquid oxygen from a semiclassical molecular dynamics simulation. *J. Phys. Chem. A* **2003**, *107*, 9070−9078.
(69) Ka, B. J.; Geva, E. Vibrational energy relaxation of polyatomic molecules in liquid solution via the linearized semiclassical method. *J. Phys. Chem. A* **2006**, *110*, 9555−9567.
(70) Ka, B. J.; Geva, E. Classical vs quantum vibrational energy relaxation pathways in solvated polyatomic molecules. *J. Phys. Chem. A* **2006**, *110*, 13131−13138.
(71) Navrotskaya, I.; Geva, E. Comparison between the Landau-Teller and flux-flux methods for computing vibrational energy relaxation rate constants in the condensed phase. *J. Chem. Phys.* **2007**, *127*, 054504.
(72) Vázquez, F. X.; Navrotskaya, I.; Geva, E. Vibrational energy relaxation rates via the linearized semiclassical method without force derivatives. *J. Phys. Chem. A* **2010**, *114*, 5682−5688.
(73) Vázquez, F. X.; Talapatra, S.; Geva, E. Vibrational energy relaxation in liquid HCl and DCl via the linearized semiclassical method: Electrostriction versus quantum delocalization. *J. Phys. Chem. A* **2011**, *115*, 9775−9781.
(74) Guo, Y.; Thompson, D. L.; Sewell, T. D. Analysis of the zero-point energy problem in classical trajectory simulations. *J. Chem. Phys.* **1996**, *104*, 576−582.
(75) Habershon, S.; Manolopoulos, D. E. Zero point energy leakage in condensed phase dynamics: An assessment of quantum simulation methods for liquid water. *J. Chem. Phys.* **2009**, *131*, 244518.
(76) Paul, A. K.; Hase, W. L. Zero-Point energy constraint for unimolecular dissociation reactions. Giving trajectories multiple chances to dissociate correctly. *J. Phys. Chem. A* **2016**, *120*, 372−378.
(77) Cotton, S. J.; Miller, W. H. The symmetrical quasi-classical model for electronically non-adiabatic processes applied to energy transfer dynamics in site-exciton models of light-harvesting complexes. *J. Chem. Theory Comput.* **2016**, *12*, 983−991.
(78) Miller, W. H.; Cotton, S. J. Classical molecular dynamics simulation of electronically non-adiabatic processes. *Faraday Discuss.* **2016**, *195*, 9−30.
(79) Tanimura, Y. Real-time and imaginary-time quantum hierarchal Fokker-Planck equations. *J. Chem. Phys.* **2015**, *142*, 144110.
(80) As a side note, the energy of the system bath interaction (V_c in eq 49) does not change very much.

DOI: 10.1021/acs.jpca.7b09018
J. Phys. Chem. A XXXX, XXX, XXX−XXX